HST.721 Hair cells and Mechanoelectric transduction

Hair Cell Locations:

Mammalian Cochlea: Inner Hair Cells, Outer Hair Cells

Mammalian Vestibular System: Type I, Type II

Non-Mammalian Vertebrate Cochleas & Vestibular Systems
    Bullfrog's Sacculus

Vertebrate Lateral Line

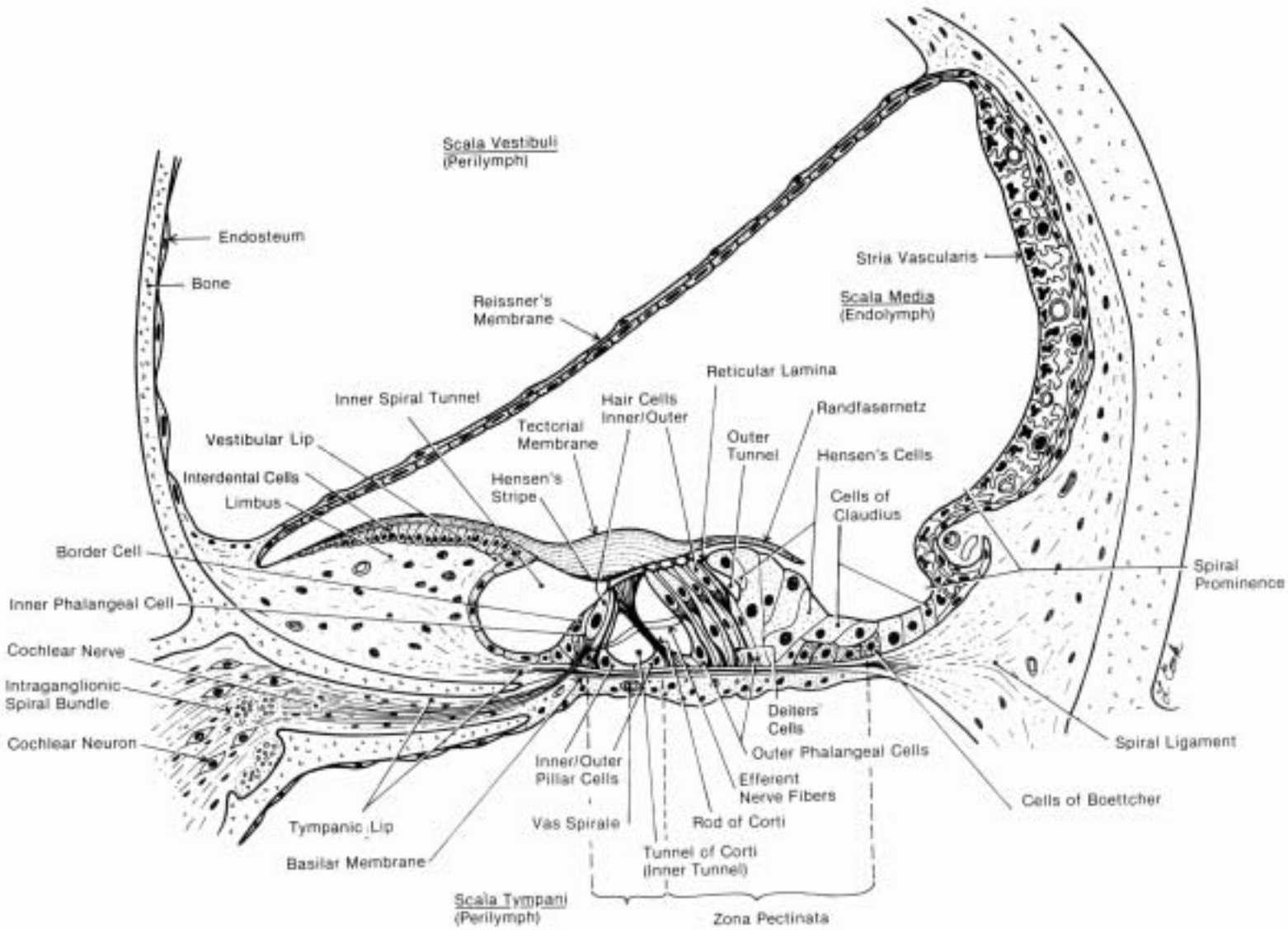
Scala Vestibuli
(Perilymph)
Endosteum
Bone
Reissner's
Membrane
Stria Vascularis
Scala Media
(Endolymph)
Reticular Lamina
Inner Spiral Tunnel
Hair Cells
Inner/Outer
Randfasernetz
Tectorial
Membrane
Outer
Tunnel
Vestibular Lip
Hensen's Cells
Interdental Cells
Hensen's
Stripe
Limbus
Cells of
Claudius
Border Cell
Spiral
Prominence
Inner Phalangeal Cell
Cochlear Nerve
Intraganglionic
Spiral Bundle
Deiters'
Cells
Cochlear Neuron
Spiral Ligament
Outer Phalangeal Cells
Inner/Outer
Pillar Cells
Efferent
Nerve Fibers
Cells of Boettcher
Tympanic Lip
Vas Spirale
Rod of Corti
Basilar Membrane
Tunnel of Corti
(Inner Tunnel)
Scala Tympani
(Perilymph)
Zona Pectinata

Hair-Cell Transduction

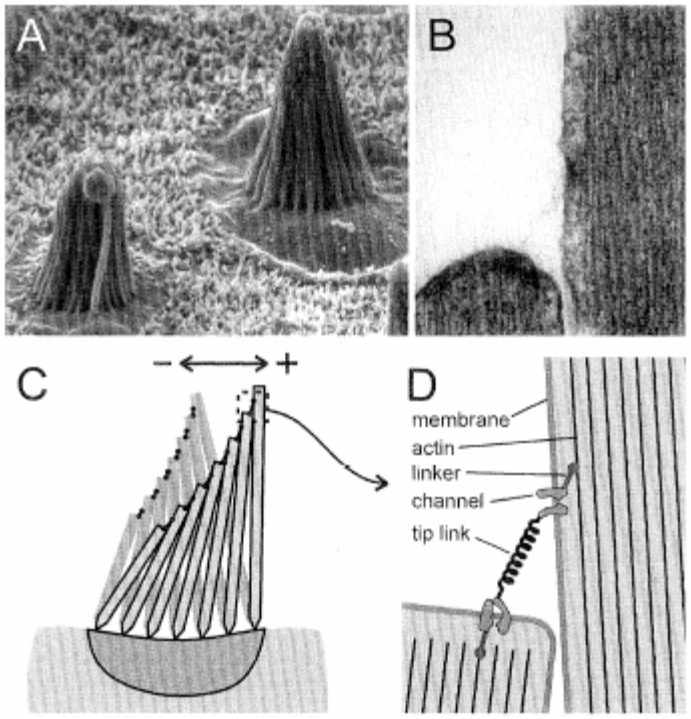

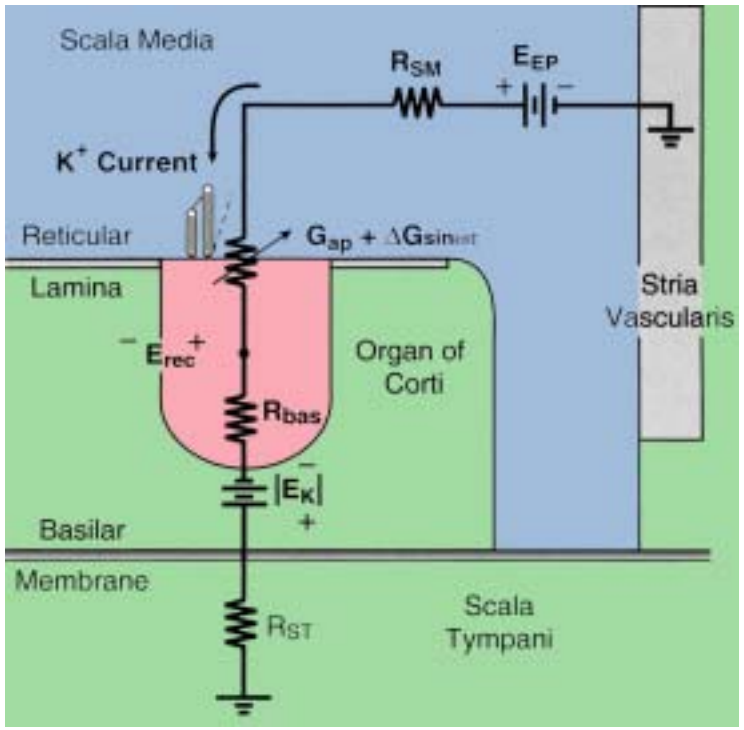

Hair Cell Directional Sensitivity, from Flock, Å. 1965. Transducing mechanisms in the lateral line canal organ receptors. Cold Spring Harbor Symp. Quant. Biol. 30, 133-145.

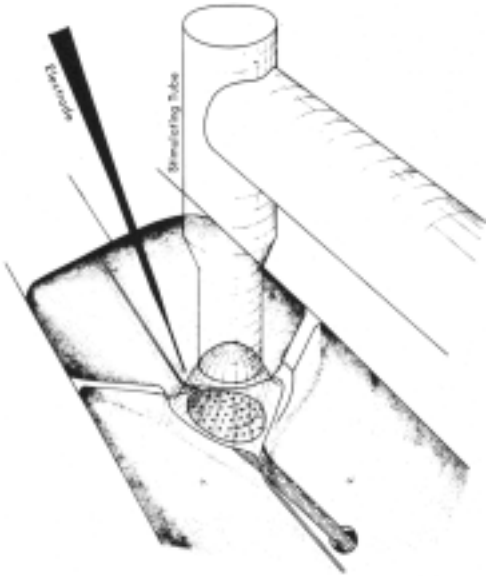

Fig. 10. Schematic drawing showing the application of the stimulating tube to the cupula and the position of the recording electrode in relation to the sensory epithelium.

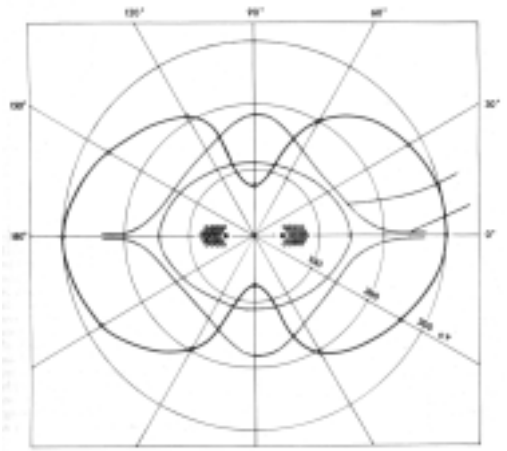

Figure 11. The directional sensitivity of an lateral line organ illustrated in a polar coordinate system. The axis of the canal is parallel to the coordinate 0^{o}-180^{o}. The outlines of the organ are indicated by the dotted line, and the orientation of the two groups of hair cells within the sensory epithelium are indicated by two sensory hair bundles oriented with their kinocilia pointing in opposite directions. The thick line is the amplitude of the microphonic potential for a vibration amplitude of 4 μm, 100 Hz.

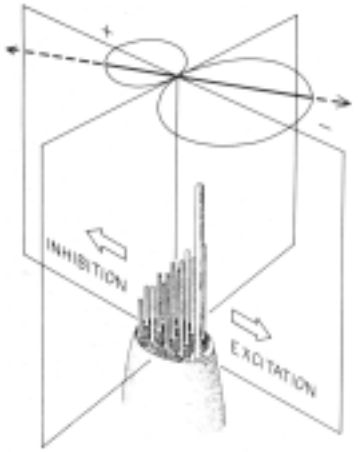

Fig. 15. The amplitude of the receptor potential is proportional to the component vector of displacement parallel to the rows of stereocilia. In the figure the receptor potential generated by equal amplitudes of cupular displacement in opposite directions is proportional to the distances cut out by the two circles. The amount of depolarization is larger than that of hyperpolarization.

Hudspeth, A.J., Corey, D.P. 1977. Sensitivity, polarity, and conductance change in the reponse of vertebrate hair cells to controlled mechanical stimuli. Proceedings of the National Academy of Sciences 74, 2407-2411.

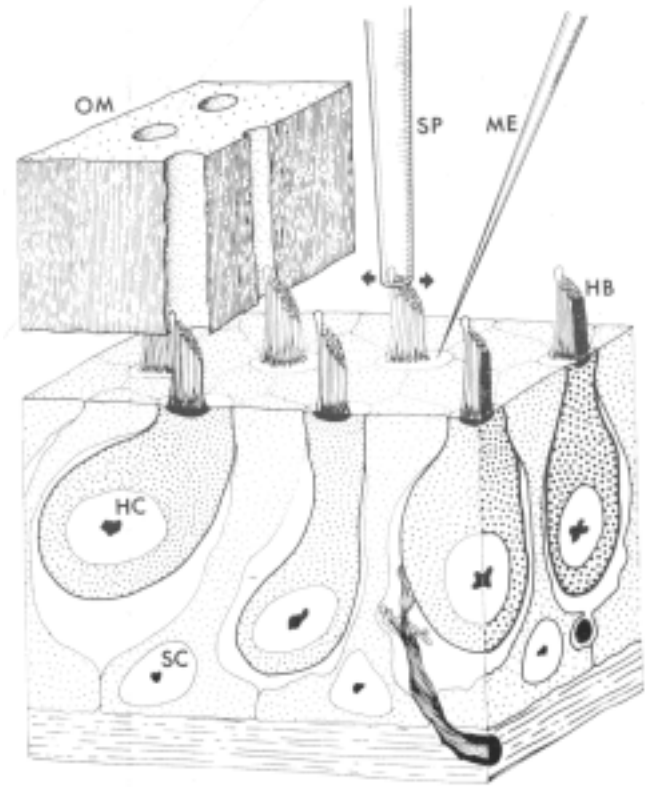

Fig. 1. Schematic cutaway of the experimental preparation. Hair cells (HC) and supporting cells (SC) form an epithelial sheet. The otolithic membrane (OM), which normally couples stimuli to the hair bundles (HB), is shown partially dissected from the site of experimentation. While the intracellular potential is recorded through a glass microelectrode (ME), a hair cell is stimulated by a capillary stimulus probe (SP) slipped over the tip of its hair bundle and moved parallel to the epithelial surface (arrows).

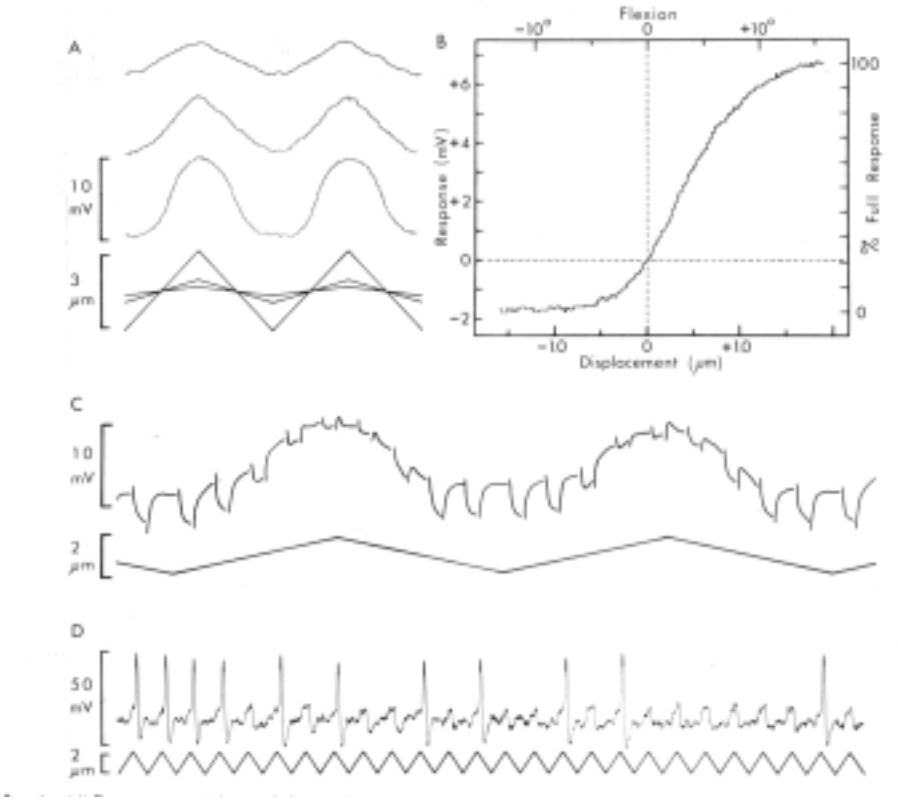

Fig. 3. (A) Receptor potential recorded from a bullfrog saccular hair cell during direct stimulation of its hair bundle. Bottom: 10-Hz triangle waves of 3 amps. Top: Resulting receptor potentials. (B) Input-output relationship for hair cell of A. The potential change from resting (-58 mV) as a function of the displacement of the hair bundle's tip by a 10 Hz triangle wave. (C) Changes in the input resistance of a hair cell during its response to mechanical stimulation. Hyperpolarizing square current pulses (70 pA, 45 msec) were injected into a cell while its hair bundle was deflected at 1 Hz (lower trace). The potential change produced by the current pulses (an index of cell input resistance), is superimposed on the receptor potential (upper trace). (D) Action potentials arising from the depolarizing phases of receptor potentials.

Corey, D.P., Hudspeth, A.J. 1979. Ionic basis of the receptor potential in a vertebrate hair cell. Nature, 675-677.

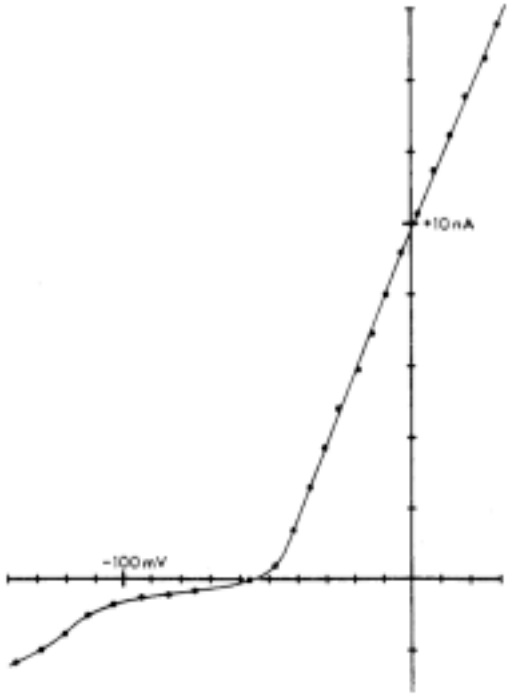

Fig. 1 Current-Voltage relationship for a saccular hair cell (no mechanical stimulation) Inward current is shown as negative. The holding potential was -60 mV. The change is slope which occurs above -50 mV probably corresponds to the "delayed rectification" of most neurons.

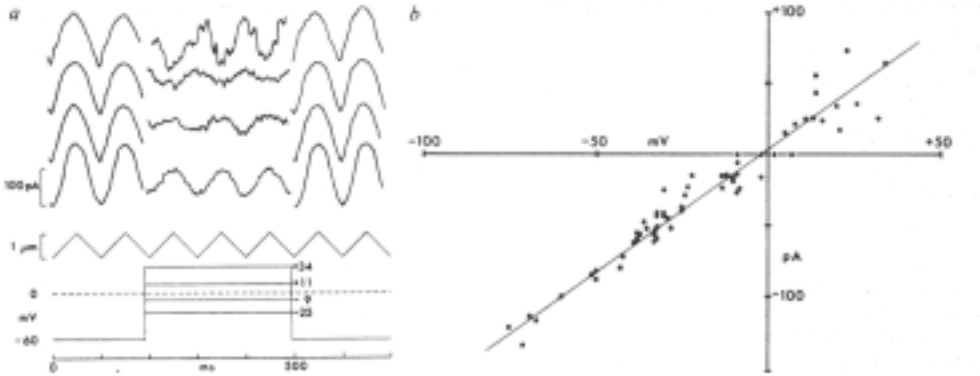

Fig. 2. a, Receptor currents at a holding potential of -60 mV and at test potentials of -25, -9, +11, and +34 mV; inward current is shown as negative. The membrane potential was held at -60 mV for 200 ms, clamped to the test potential for 300 ms, and returned to the holding potential. The hair bundle was continually moved with a 1.1 μm, 10-Hz, triangle-wave stimulus, shown below the current records; downward represents a deflection toward the kinocilium. B, Magnitude of the receptor current as a function of membrane potential; normalized data from 24 cells. The line is a linear regression to fit the data (r^2=0.97); its zero-current intercept, the reversal potential, is -2 mV. The external fluid was standard, high-Na^+ saline, so that the reversal potential is not the equilibrium potential of Na^+, K^+, or Ca^{2+}.

Other data show that the transduction channel is nonspecific and is permeable to Li^+, Na^+, K^+, Rb^+, Cs^+, Ca^{2+}, and at least one small organic cation.

Hudspeth, A.J. 1982. Extracellular current flow and the site of transduction by vertebrate hair cells. J. Neurosci. 2, 1-10.

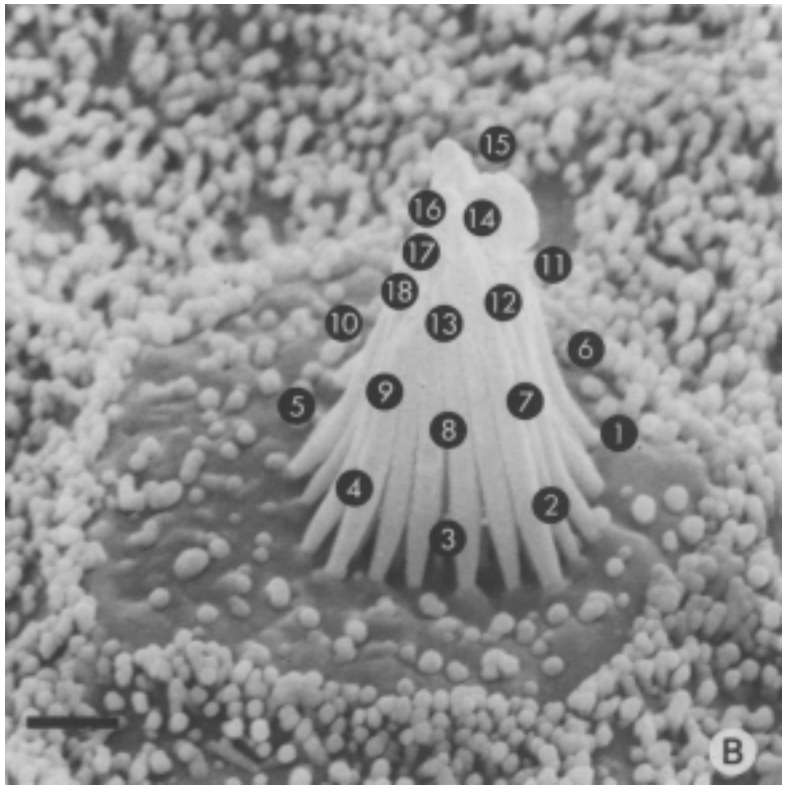

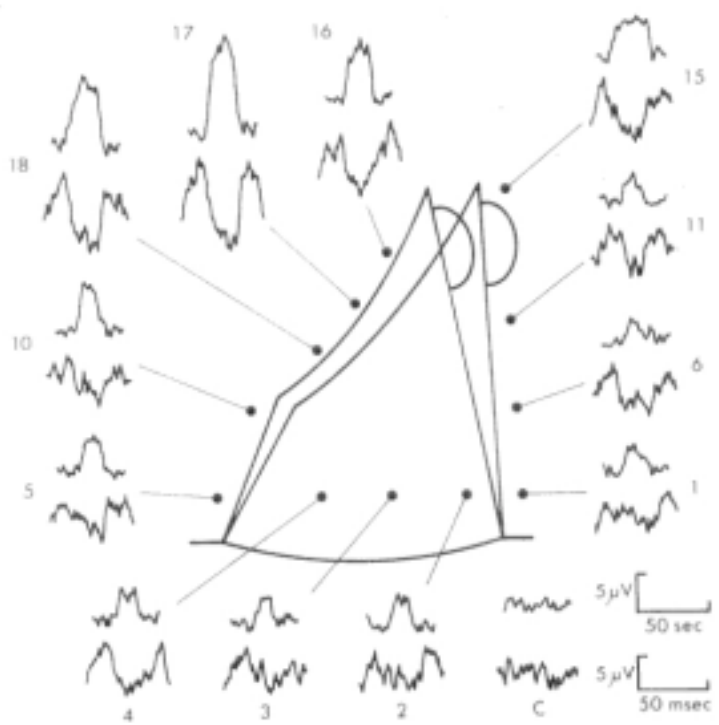

Extracellular Voltage
(microVolts P-P)

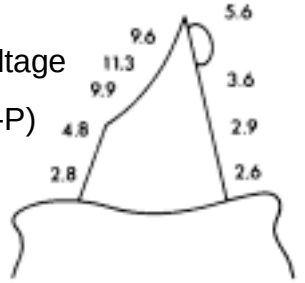

Pickles, J.O., Comis, S.D., Osborne, M.P. 1984. Cross-links between stereocilia in the guinea pig organ of Corti, and their possible relation to sensory transduction. Hear Res 15, 103-12.

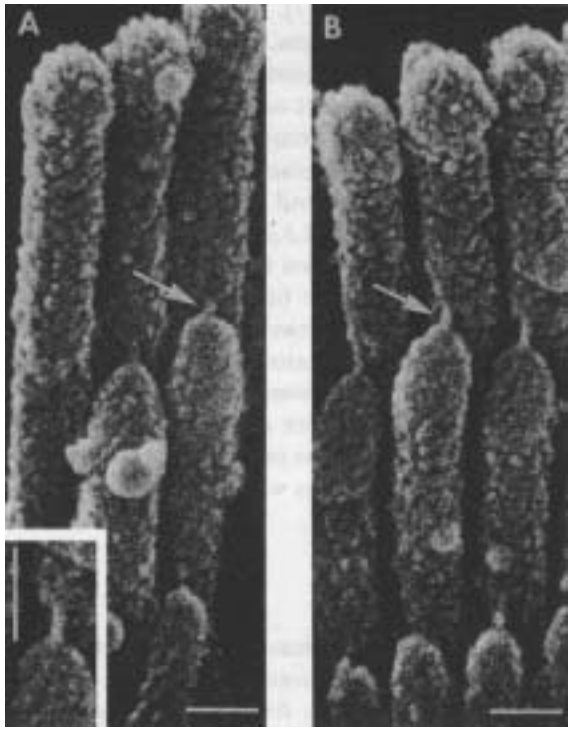

Fig. 2. Links (arrows) stretching upwards from the tips of the shorter stereocilia to their taller neighbors in the next row, on an outer hair cell. Each shorter stereocilium gives rise to only one link of this set. (A) The stereocilia at the end of the V-shaped row on an outer hair cell: the upward-pointing links run away from the end of the row and so away from the modiolar side of the hair cell. (B) The stereocilia of the same hair cell, halfway between the tip and the apex of the 'V'. The inset shows an upwards-pointing link at a greater magnification. Bars: 100 nm.

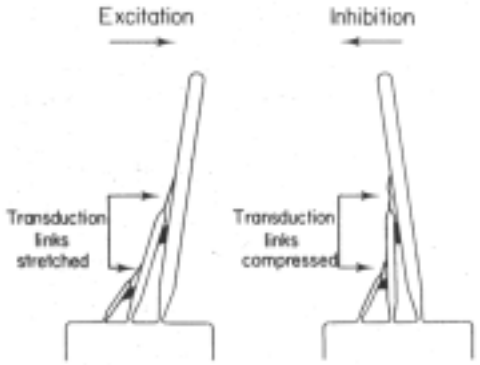

Fig. 9. A hypothesis of transduction in hair cells, based on the present observations. The lateral links hold the tips of the shorter stereocilia against the longer stereocilia. When the bundle of stereocilia is deflected, a vertical shear is produced between the rows which is detected by the single upwards-pointing link, running from the tip of each shorter stereocilium. It is suggested that stretch of the link decreases the membrane resistance.

Denk, W., Holt, J.R., Shepherd, G.M.G., Corey, D.P. 1995. Calcium imaging of single stereocilia in hair cells: Localization of transduction channels at both ends of tip links. Neuron 15, 1311-1321.

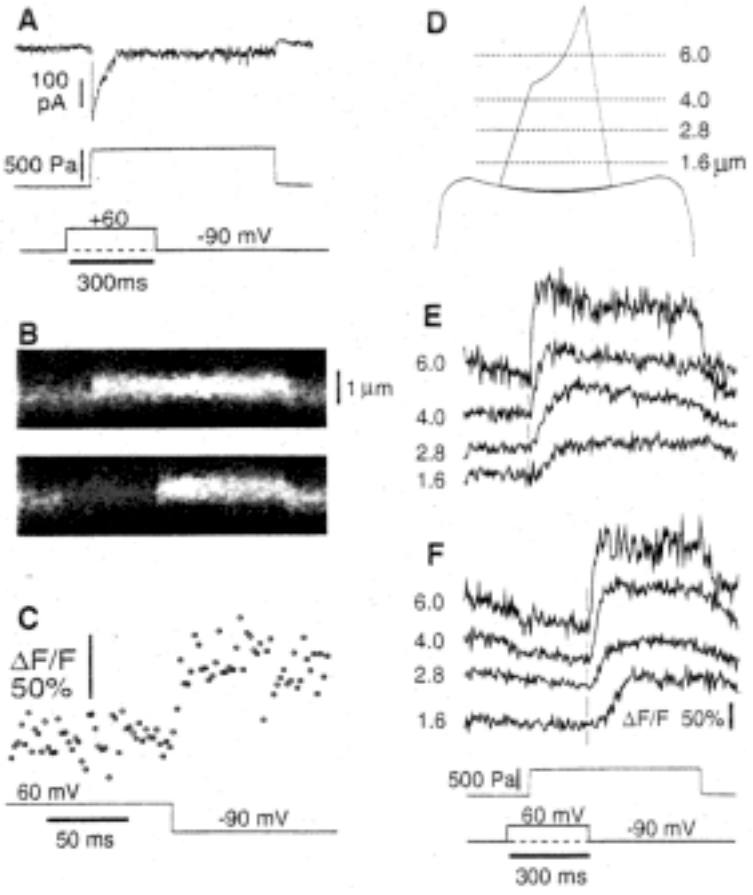

Fig. 4. Time Course of Calcium Signal at Different Heights in a Bundle.

(A) A 600 Pa pressure step was delivered to the back of the fluid-jet pipette, causing a bundle deflection of ~0.5 µm that elicited a 250 pA receptor current. The pressure step protocol applies to (A). Both protocols apply to (B).

(B) Line scan through the tip of the bundle, at ~7.0 µm above the apical surface. For the upper image, the bundle was deflected for 600 ms with a constant holding potential of -90 mV. For the lower image, the holding potential was depolarized to +60 mV for 300 ms, beginning 100 ms before the deflection. In both images, the deflection can be seen in the movement of the bright region.

(C) Intensity as a function of time, for a plane ~7.0 mm above the apical surface. Each scan line in B (lower image) was integrated, to calculate a spatially averaged intensity every 2 ms. The flourescence intensity was plotted as a proportional increase over the resting value. ΔF/F. The command potential is shown at bottom.

(D) Illustration of the image planes for E and F.

(E) Change in CG-1 fluorescence as a function of time, in the case without a depolarization, for the four planes shown in (D). The stimulus protocol is shown at bottom in (F).

(F) Change in CG-1 fluorescence, in the case with a depolarization.

Holt, J.R., Corey, D.P. 2000. Two mechanisms for transducer adaptation in vertebrate hair cells. Proc Natl Acad Sci U S A 97, 11730-5.

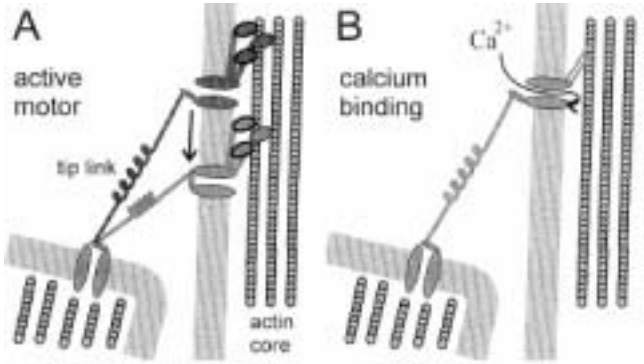

Fig. 3. (A) Schematic diagrams illustrating the two models for hair cell adaptation. (A) The active motor model proposes that when the bundle is deflected in the positive direction, the motor cannot resist the increased tension and slips down the stereocilium, reducing tension and allowing channels to close. In addition, Ca2+ entry through open channels accelerates the rate of slipping. Conversely, when the bundle is deflected in the negative direction, the reduced tension allows the motor to climb and restore tension to reopen channels. (B) The calcium-dependent closure mechanism proposes that when the channels open, calcium enters the stereocilia and binds to a site on or near the channel protein. Bound Ca^{2+} promotes a closure of the channel. When deflected in the negative direction, the Ca^{2+} concentration falls and reduces the inhibition of the channel.

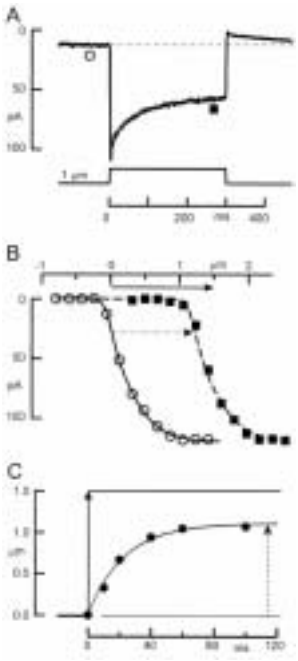

Fig. 2. Properties of adaptation in a mouse utricular type II hair cell. (A) Transduction current from a step displacement of the hair bundle. (B) The current-displacement, I(x), relation shifts in the direction of the applied stimulus. Circle & box from the times indicated in A. (C) Magnitude of the I(x) shift as a function of time.

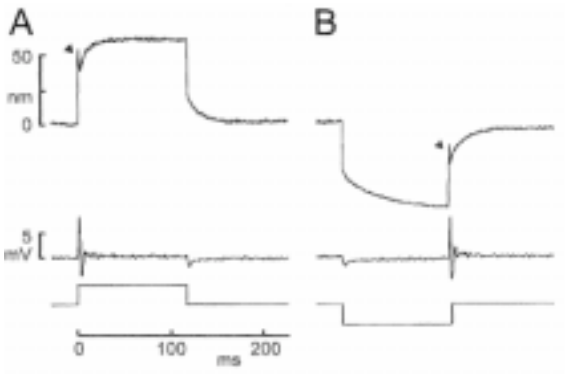

Fig. 4. The “twitch” and subsequent slow relaxations of the hair bundle during maintained force steps. (A) A positive force caused a quick forward deflection of ~50 nm (arrowhead), a rapid twitch back of ~10 nm, and then a relaxation forward of ~25 nm. The receptor potential recorded simultaneously (middle trace) showed a transient depolarization, and then an oscillation during and after the twitch. (B) A negative force evoked a quick negative deflection and slower negative relaxation. The twitch was not observed until the bundle was returned to the rest position (arrowhead) and was associated with an oscillation.

Howard, J., Hudspeth, A.J. 1987. Mechanical relaxation of the hair bundle mediates adaptation in mechanoelectrical transduction by the bullfrog's saccular hair cell. Proc. Natl. Acad. Sci. USA 84, 3064-3068.

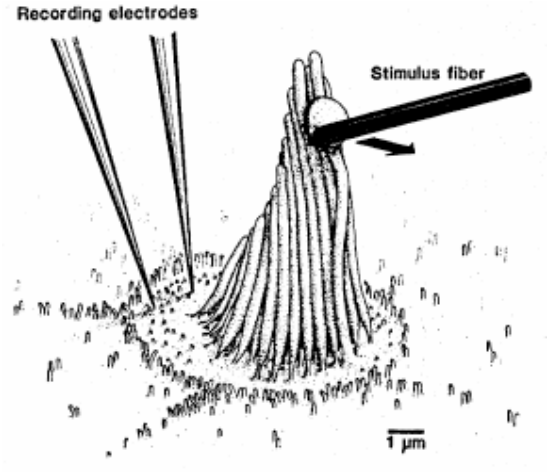

Fig. 1 Diagram of the apical surface of a saccular hair cell. Movement of the base of the flexible fiber forced the hair bundle to undergo a displacement. Positive deflection indicated by arrow. Two electrode voltage clamp: One electrode to record voltage and one to pass current.

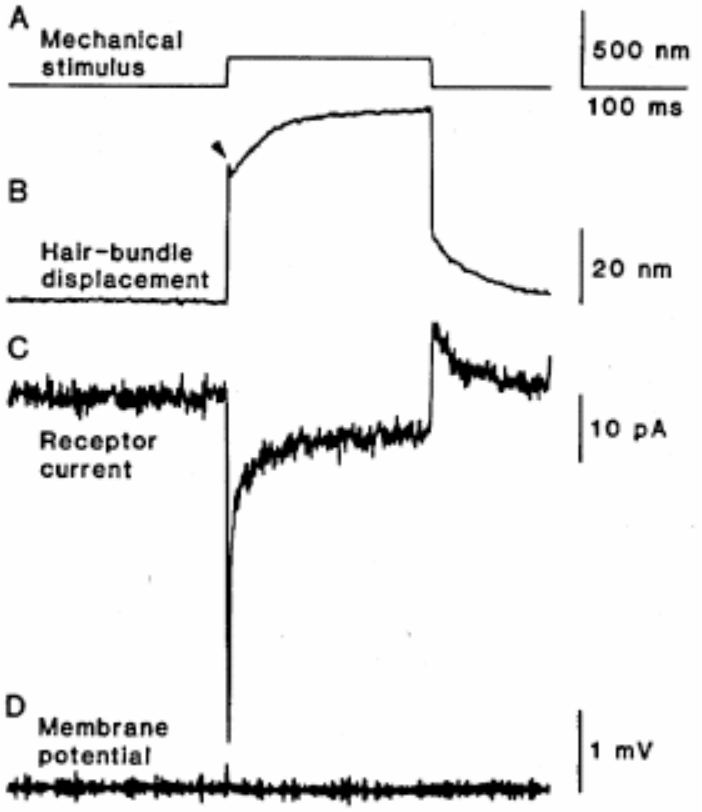

Fig. 2. Simultaneous mechanical and receptor-current responses to a force step. (A) The base of the fiber was given a 186-nm positive step displacement. (B) The bundle underwent an abrupt initial displacement followed by a slow relaxation. The notch in the bundle displacement (arrowhead) was seen in many instances. (C) The current measured simultaneously with a voltage clamp had an initial, fast, inward transient followed by a slower adaptation. An overshoot and slow adaptation occurred at the end of the step. The two components of adaptation in the receptor current had time courses similar to those of the mechanical relaxations. (D) The cell's membrane potential was effectively clamped at -70 mV. The stiffness of the force fiber was 340 µN/m.

Assad, J.A., Hacohen, N., Corey, D.P. 1989. Voltage dependence of adaptation and active bundle movement in bullfrog saccular hair cells. Proc Natl Acad Sci U S A 86, 2918-22.

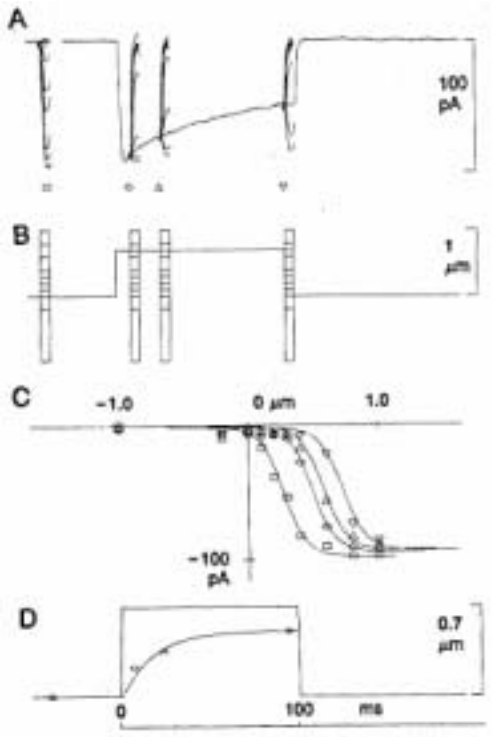

Fig. 2. Shift of current-displacement, I(x), curve during a maintained displacement at -80 mV. (A) Superimposed responses to 10 stimulus presentations. (B) The stimulus: a maintained displacement of 0.7 mm for 100 ms and one short test step of varying amplitude and time. (C) I(x) curves from responses to test steps at different times. (D) Amplitude of the shift measured at the midpoint of the sigmoidal curves, vs. time. The time constant of the shift was 17.4 ms.

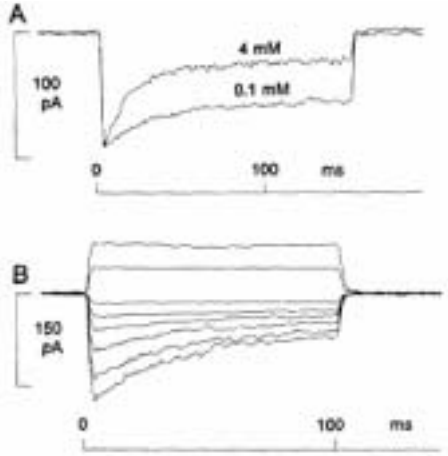

Fig. 3. Calcium and voltage dependence of adaptation. (A) The decline in current, indicating the rate of adaptation, was greater in high (4 mM) than in low (0.1 mM) calcium saline (0.5 μm step). High calcium partially blocked the transduction current; so the trace in 4 mM calcium was scaled to match the peak current in 0.1 mM calcium. (B) The decline was also faster at hyperpolarized potentials. Membrane potential was changed to a new value 300 ms before the mechanical stimulus (0.7 μm step) and held for the duration of the trace. Test potentials (from top trace down): +90, +60, +10, -10,-30,-60,-90,& -110 mV. Traces were aligned so that resting currents at each potential were superimposed.

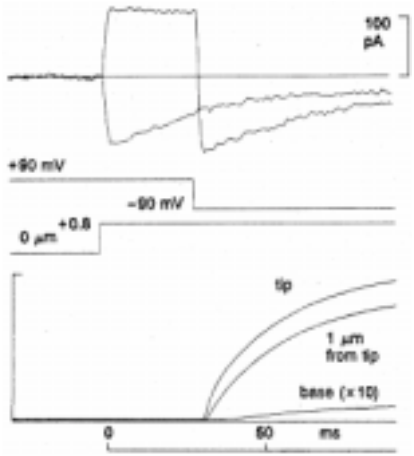

Fig. 6. Time course of calcium action. Membrane potential was held at +90 mV for 300 ms preceding a 0.5 mm stimulus and then changed to -90 mV, 30 ms after the start of the mechanical stimulus. Membrane potential was held continuously at -90 mV in the control trace. The time course of intracellular calcium concentration change predicted from a simple diffusion model is shown in the bottom trace for the tip of a stereocilium, 1 μm from the tip, and at the base (where it is expanded by a factor of 10).

Also, they saw motion (32+/-14 nm) of the stereocilia due to changing the voltage from -80 mV to +80 mV.

Fettiplace, R., Ricci, A.J. 2003. Adaptation in auditory hair cells. Curr Opin Neurobiol 13, 446-51.

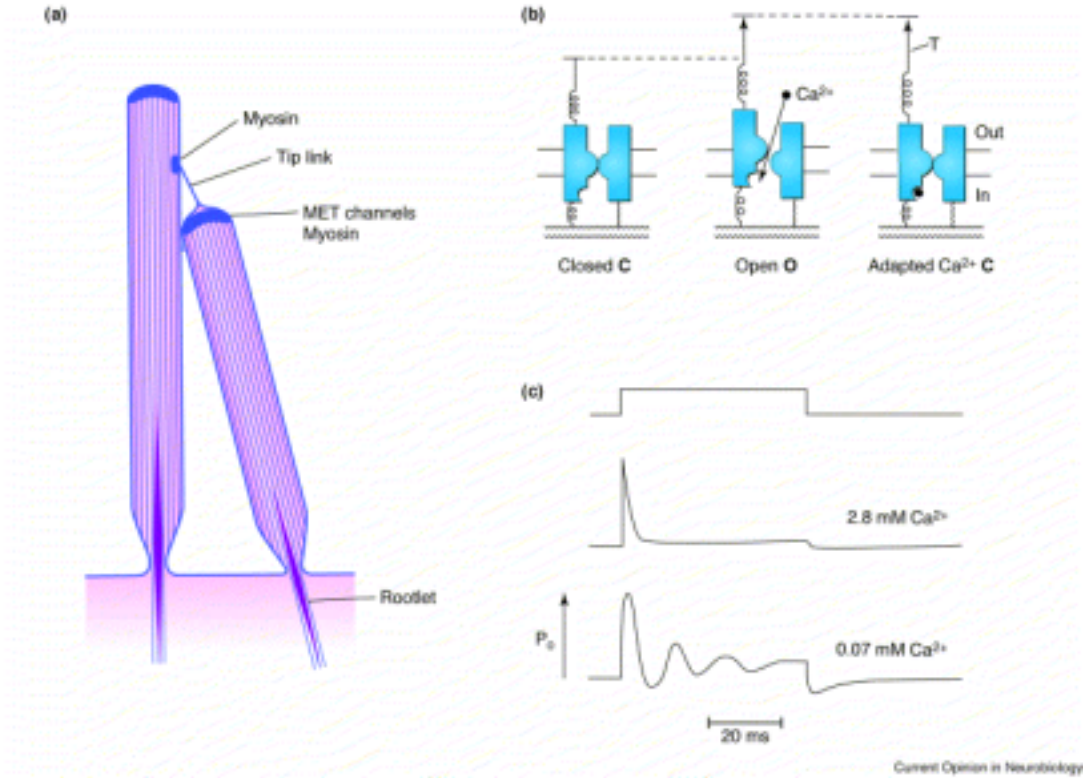

Fig. 1. Sites and action of hair cell adaptation (a) Structural components of the stereocilia associated with transduction and adaptation, showing the electron dense plaques that represent sub-membranous protein complexes. Rotation towards the taller stereocilium exerts force on the tip link and opens MET channels at the stereociliary tip. Tension in the tip link may be adjusted adaptively by myosin arrays (1c, 7a or 15) at either end of the tip link; for example, myosin-1c in the upper plaque tensions the link by climbing up towards the barbed end of the actin filaments. Stereociliary position could also be influenced by the stiffness of the rootlets into the hair cell apex. (b) Hair bundle displacement tensions the tip link (T) which extends the internal and external gating springs causing the channel to go from the closed (C) to the open (O) configuration. Ca^{2+} entering the stereocilium through the open channel binds at the inner face of the channel and shuts it. This generates force by increasing tension in the gating springs. (c) Following a bundle deflection (top), the channel opens rapidly then recloses adaptively in a high concentration of 2.8 mM Ca^{2+}. Change in p_o is plotted against time. When the extracellular Ca^{2+} concentration is reduced to 0.07 mM Ca^{2+}, a more realistic physiological value closer to that in cochlear endolymph, the adaptation becomes oscillatory at 77 Hz. The resonant frequency of the MET channel varies with hair cell CF.

Martin, P., Mehta, A.D., Hudspeth, A.J. 2000. Negative hair-bundle stiffness betrays a mechanism for mechanical amplification by the hair cell. Proc Natl Acad Sci U S A 97, 12026-31.

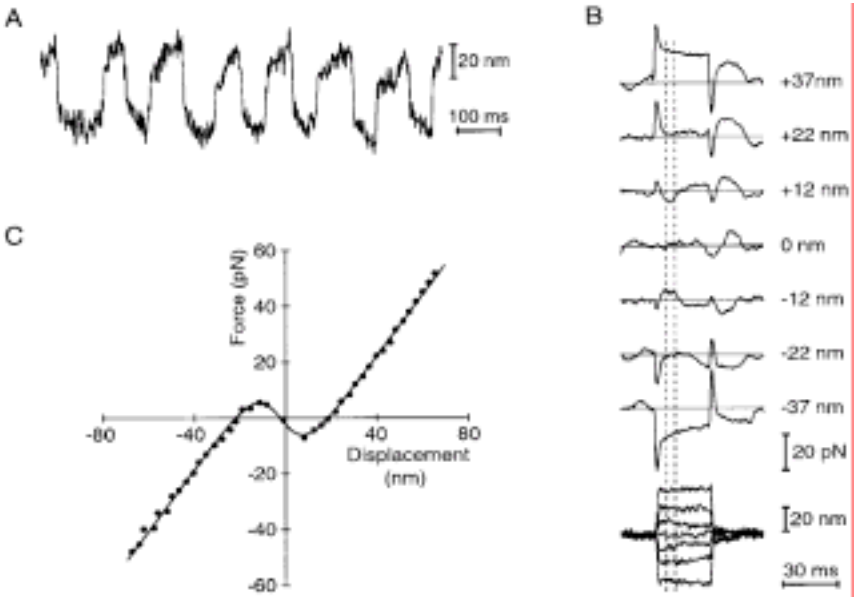

Fig. 1. (A) Spontaneous oscillation at ~7 Hz of a hair bundle from the bullfrog's sacculus. (B) The relation between hair-bundle displacement (lower family of traces) and applied force (upper traces) under displacement clamp conditions. (C) Displacement-force relation measured under displacement-clamp conditions. Each point represents a bundle displacement and the corresponding force exerted by the fiber, as averaged over the time window designated in B.

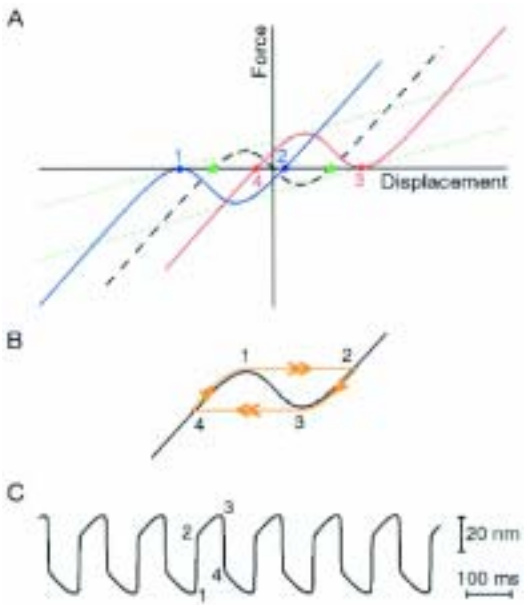

Fig. 3. A model of the hair bundle's spontaneous oscillation. (A) Force-displacement relations at different times during a spontaneous movement. Green stars indicate

(B) Trajectory (1->2->3->4) of the hair bundle along the displacement-force relation as this relation undergoes the adaptive shift depicted in A. Double arrows indicate fast transitions across the unstable region of negative stiffness; single arrows demarcatge slow adaptive movements along the stable branches of the relation. (C) Hair-bundle oscillation produced by a model of bundle mechanics with parameter values for the cell in Fig. 1A. The numbers relate phases of the oscillation to points on the displacement-force relations of A and B.

Hair-Cell Transduction

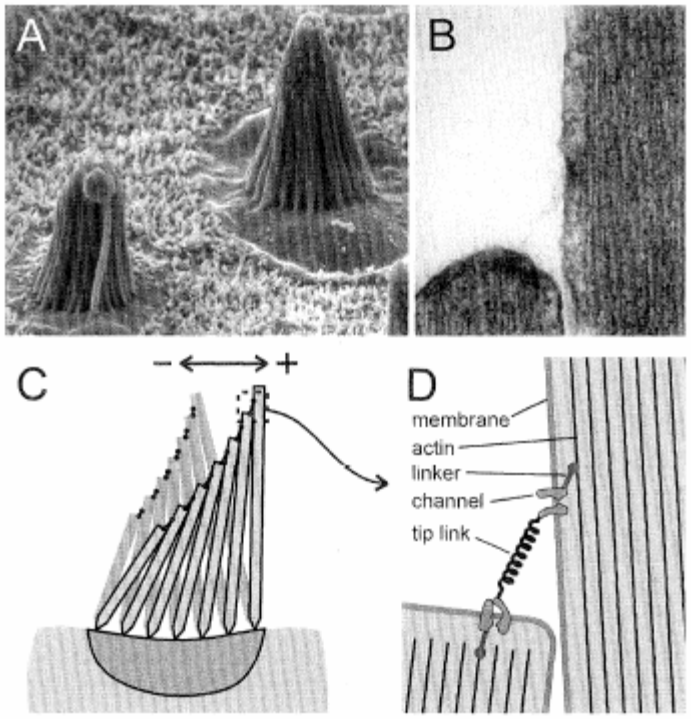

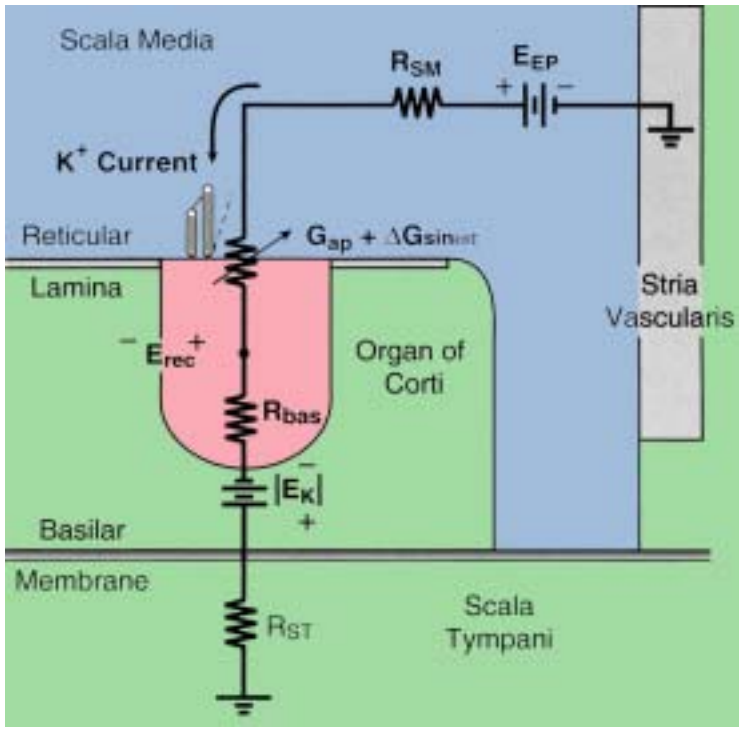

Hair Cell Receptor Potential vs. Frequency